ADVANCES IN ATMOSPHERIC SCIENCES, VOL. 21, NO. 5, 2004, 784–801

A Possible Feedback Mechanism Involving the Arctic Freshwater, the Arctic Sea Ice, and the North Atlantic Drift

Odd Helge OTTERÅ*[1,2] and Helge DRANGE[1,2,3,4]

[1] *Nansen Environmental and Remote Sensing Center, Edv. Griegsvei 3A,5059 Bergen*

[2] *Bjerknes Centre for Climate Research, Allégt. 55, 5007 Bergen*

[3] *Geophysical Institute, University of Bergen, Allégt. 70, 5007 Bergen*

[4] *Nansen-Zhu International Research Centre, Beijing* 100029

(Received 19 November 2003; revised 15 March 2004)

ABSTRACT

Model studies point to enhanced warming and to increased freshwater fluxes to high northern latitudes in response to global warming. In order to address possible feedbacks in the ice-ocean system in response to such changes, the combined effect of increased freshwater input to the Arctic Ocean and Arctic warming—the latter manifested as a gradual melting of the Arctic sea ice—is examined using a 3-D isopycnic coordinate ocean general circulation model. A suite of three idealized experiments is carried out: one control integration, one integration with a doubling of the modern Arctic river runoff, and a third more extreme case, where the river runoff is five times the modern value. In the two freshwater cases, the sea ice thickness is reduced by 1.5–2 m in the central Arctic Ocean over a 50-year period. The modelled ocean response is qualitatively the same for both perturbation experiments: freshwater propagates into the Atlantic Ocean and the Nordic Seas, leading to an initial weakening of the North Atlantic Drift. Furthermore, changes in the geostrophic currents in the central Arctic and melting of the Arctic sea ice lead to an intensified Beaufort Gyre, which in turn increases the southward volume transport through the Canadian Archipelago. To compensate for this southward transport of mass, more warm and saline Atlantic water is carried northward with the North Atlantic Drift. It is found that the increased transport of salt into the northern North Atlantic and the Nordic Seas tends to counteract the impact of the increased freshwater originating from the Arctic, leading to a stabilization of the North Atlantic Drift.

Key words: Arctic Ocean, freshwater, seaice, North Atlantic Drift

1. Introduction

It is believed that the transport of freshwater into the high northern oceans plays a major role in the circulation in the Nordic Seas and the Atlantic (and possibly the World) Ocean since it passes convective regimes of major importance to the thermohaline circulation (Aagaard and Carmack, 1989). The role of high latitude freshwater input is of particular interest from a paleo perspective. The response of the ocean circulation to increased meltwater fluxes during the last deglaciation (14–15 kyr BP) can possibly explain the highly variable climate during this period (e.g., Broecker et al., 1992; Lahman and Keigwin, 1992; Clark et al., 2002).

Simonsen (1996) computed the meltwater fluxes into the Atlantic Ocean, the Nordic Seas, and the Arctic Ocean based on the paleo-topography reconstruction of Peltier (1994). The obtained 1000-year mean meltwater flux into the Nordic Seas and the Arctic Ocean was comparable with the modern freshwater input of 0.1 Sv (1 Sv=10^6 m^3 s^{-1}; Aagaard and Carmack, 1980) during the last deglaciation. However, paleo data records indicate that the major melting lasted only 300–500 years (Fairbanks, 1989; Jones and Keigwin, 1988), implying freshwater fluxes 2–3 times larger than the 1000-year mean during the major melting events.

Fully coupled atmosphere-sea ice-ocean climate models are currently used to examine the past, present, and possibly future climate states. The present day climate models give a fairly representative picture of sev-

*E-mail: oddho@nersc.no

eral aspects of the current climate system (e.g., Latif, 1998; Cooper and Gordon, 2002; Furevik et al., 2003). Many state-of-the-art climate models show a 20%–30% reduction in the Atlantic Meridional Overturning Circulation (AMOC) when forced with greenhouse gas and aerosol projections for the current century (e.g., Cubasch et al., 2001).

A typical and quite robust response in coupled model simulations is increased evaporation at low latitudes, and increased precipitation and continental runoff to the high northern latitudes. It is therefore tempting to believe that an increased supply of freshwater and warming at high northern latitudes will lead to reduced formation rates of intermediate and deep water masses, and consequently to a reduced AMOC (Peterson et al., 2002). However, a different model response was identified by Latif et al. (2000). Here, large-scale air-sea interactions in the Tropics, with a pattern similar to a strong and persistent El Niño (Timmermann et al., 1998), led to anomalously high salinities in the tropical Atlantic. These anomalies were then advected northward into the convective regions of the North Atlantic, thereby compensating for the effect of local warming and freshening. Also other model experiments show essentially no changes in the AMOC during the 21st century (Gent, 2001; Sun and Bleck, 2001).

In addition to increased surface freshwater fluxes at the high northern latitudes, most climate models show an enhanced greenhouse warming in the polar regions, especially for the Arctic, with a predicted warming of 3–4°C during the next 50 years (Mitchell et al., 1995; Räisänen, 2001). This will most likely lead to changes in both the extent and the thickness of sea ice in the Arctic, with consequences for the Arctic region (Vinnikov et al., 1999; Johannessen and Miles, 2000).

Here we address these questions by exploring the isolated effects of increased freshwater input to the Arctic Ocean and Arctic warming—the latter manifested as a gradual reduction in the sea ice thickness—by means of idealized model experiments. For the experiments, an isopycnic coordinate ocean general circulation model (OGCM) fully coupled to a dynamic-thermodynamic sea ice model has been used (see section 2). The model experiments are described in section 3 and the results of the control and perturbed simulations are provided in sections 4 and 5, respectively. The obtained results are discussed in section 6, and the findings are summarized in section 7.

2. The coupled ocean-sea ice model

The OGCM applied in this study is based on the Miami Isopycnic Coordinate Ocean Model (MICOM) (see Bleck et al., 1992 for a thorough desription of the model). To describe the high latitude climate system, dynamic and thermodynamic sea ice modules have been coupled to MICOM (Drange and Simonsen, 1996). The sea ice module modifies the heat and freshwater fluxes between the ocean and the atmosphere by freezing or melting ice in order to prevent the sea surface temperature to decrease below the freezing point of sea water. If ice is present and the sea surface temperature increases, ice is melted in order to keep the sea surface temperature at the freezing point. The dynamic ice model, which transports ice as a result of the applied wind field and the simulated surface currents and sea surface tilt, is based on the classical viscous-plastic rheology of Hibler (1979) but in the modified implementation of Harder (1996).

For this study a regional version of MICOM has been adopted. The model domain includes the Atlantic Ocean north of 20°S and the entire Arctic Basin (Fig. 1). A locally orthogonal curvilinear horizontal grid (Simonsen and Drange, 1997) was adopted with grid focus in the Nordic Seas with a maximum grid resolution of about 40 km. Artificial (closed) boundaries occur south of the Bering Strait, along the South Atlantic boundary, and in the Strait of Gibraltar.

The model was initialized with temperature and salinity fields for September from the National Oceanographic Data Center (Levitus et al., 1994; Levitus and Boyer, 1994), and is forced by monthly mean climatologic atmospheric fields. The wind stress and absolute wind speed were derived from the European Centre for Medium Range Weather Forecasts (ECMWF, 1988), merged with data from the Comprehensive Ocean Atmosphere Data Set (COADS) in the central Atlantic Ocean (Oberhuber, 1988; Aukrust and Oberhuber, 1995). Cloud cover and relative humidity are from COADS, with data from Huschke (1969) and Maykut (1978) respectively, included in the central Arctic. The air temperature is from COADS, but with data from ECMWF and coastal weather stations in ice covered regions as prepared by Simonsen and Haugan (1996). Precipitation is derived from Legates and Willmott (1990).

The model bathymetry is computed as the arithmetic mean of the 5-min resolution ETOPO5 database (NOAA, 1988). The continuity, momentum, and tracer equations are discretized on an Arakawa C-grid stencil (Arakawa and Lamb, 1977), implying that water transport will take place in channels or openings with a width of one single grid cell. In the model configuration used here, the Canadian Archipelago has been included as a 250 m deep channel between the North American continent and Greenland. For model systems with higher horizontal resolution, a more realistic representation of the Canadian Archipelago can and should be made. For the resolution common to most climate models, the approach adopted here is straightforward and represents a simple (although not

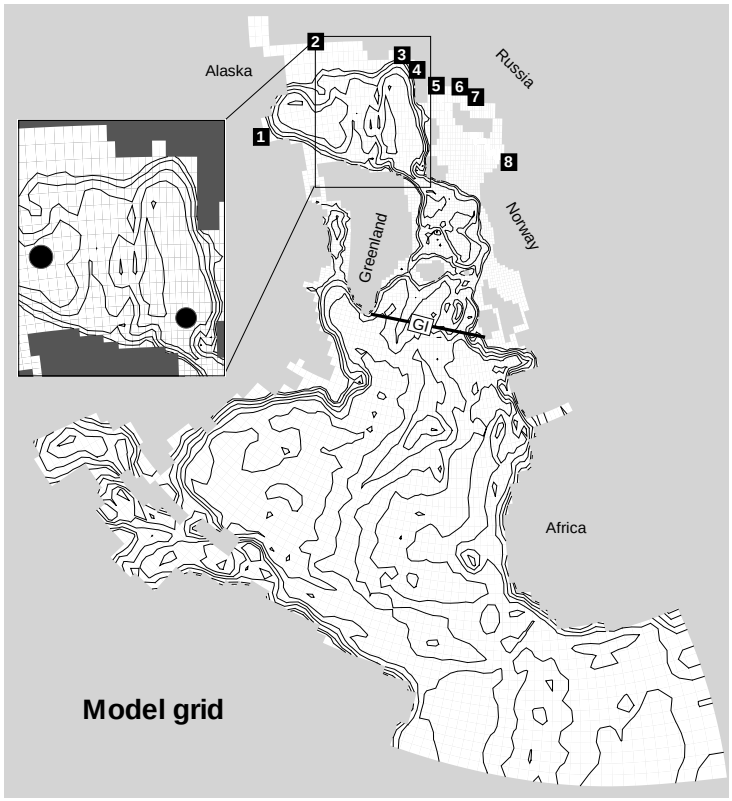

Fig. 1. The model grid used in this study. The numbers 1–8 represent the major river discharge locations in the Arctic Ocean (MacKenzie, Kolyma, Kotuy, Lena, Ob, Yenisei, Pyasina, and Northern Dvina, respectively). Also shown are two locations in the Arctic Ocean that are mentioned in the text, one in the Eurasian Basin and a second one in the Canadian Basin. Finally, the Greenland-Ireland transect used in the text is shown.

perfect) representation of, for instance, the Canadian Archipelago. Note that for models applying an Arakawa B-grid stencil, two grid cells are needed to resolve transport through channels or openings.

All the major rivers in the model domain are included. The seasonal variation in the river output is adopted from Dümenil et al. (1993). For those rivers where the seasonal variation is unknown, the variation from a neighboring river is used. The annual mean river discharge is adopted from Aagaard and Carmack (1989), Dümenil et al. (1993), Mosby (1962), and Semtner (1987), and amounts to about 0.1 Sv for the Arctic rivers (the locations of the major Arctic rivers are indicated in Fig. 1). A virtual salt flux formulation is used for the river runoff in the model (fixed ocean volume and no volume flux). Therefore, no additional mass of water is added through river runoff. Since the virtual salt flux formulation cannot conserve the ocean salt content (Roullet and Madec, 2000), a restored sea surface salinity (SSS) is used to limit the surface salinity drift.

The model was first spun up for 40 years. This is too short to draw any definite conclusions about the model performance. However, at this point an annual steady state circulation was achieved, and the main features of the circulation in the Arctic Ocean and the Nordic Seas were reproduced. During the spin-up, relaxation of sea surface temperature (SST; Levitus and Boyer, 1994) and SSS (Levitus et al., 1994) was applied. Since there are few hydrographic observations from the Arctic, relaxation of SST was switched off wherever the monthly sea ice climatology by Walsh and Johnson (1979) showed ice, whereas relaxation of SSS was made towards the annual mean salinity field of the area. After the spin up period of 40 years, the model was run for another three years with continued relaxation applied to temperature and salinity. During this period, the SSS fluxes implied by the SSS relaxation were diagnosed and monthly mean values were computed and stored.

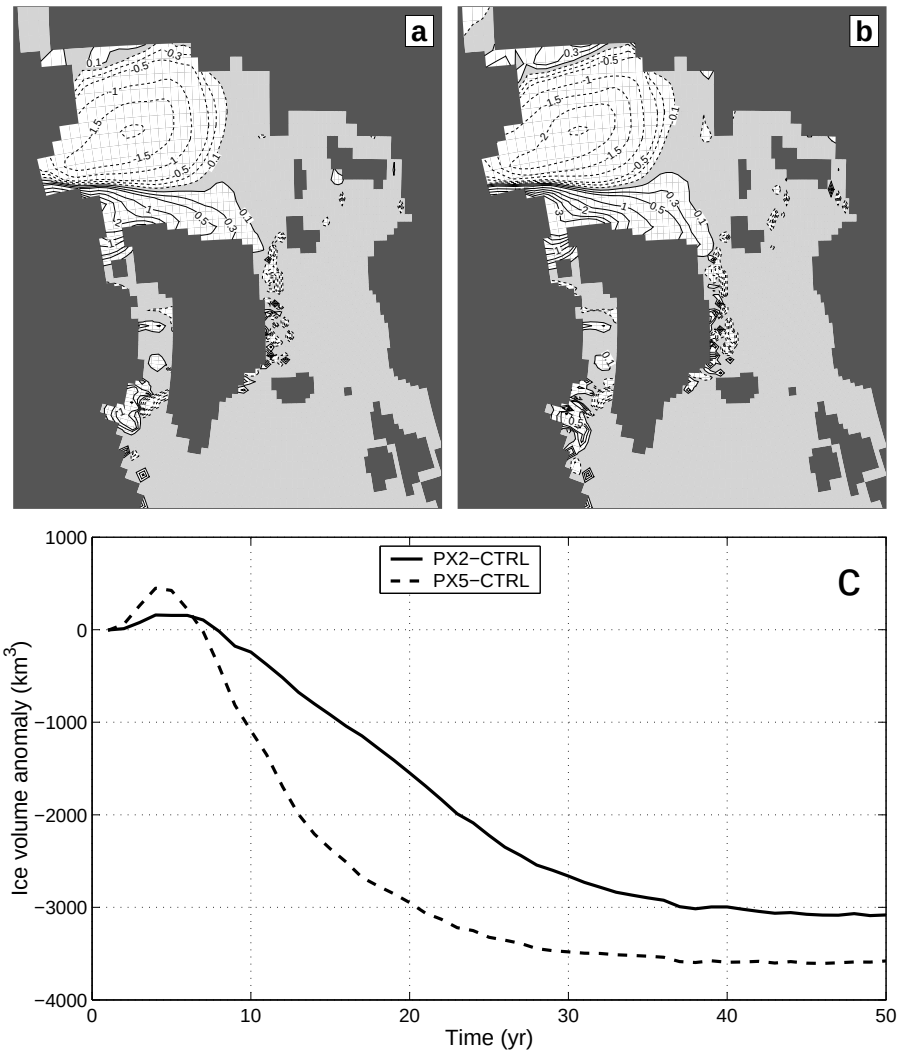

Fig. 2. Changes in the sea ice thickness (m) for March in year 50. (a) PX2−CTRL and (b) PX5−CTRL. Contour interval is 0.5 m. In addition, the ±0.3 m and ±0.1 m contour levels are shown. (c) Temporal changes in the sea ice volume (km^3) for March in the central Arctic Ocean.

A total of three 50-year simulations were then carried out (see below). During the three model experiments, the diagnosed monthly mean SSS fluxes were used as flux forcing for salinity in order to let SSS anomalies freely develop, propagate, and decay in the model, while standard relaxation was used for SST.

3. Design of the freshwater experiments

All of the 19 climate models participating in the Coupled Models Intercomparison Project CMIP-2 predict increased precipitation and enhanced warming in the high northern latitudes in response to increased greenhouse gas forcing (Räisänen, 2001). The magnitude of the increase in precipitation depends on the model (Räisänen, 2001), and likely on the strength of the applied greenhouse gas forcing. For instance, in the transient greenhouse warming simulation by Latif et al. (2000), an increased surface freshwater flux (precipitation minus evaporation plus river runoff) of 0.1 Sv was found poleward of 45°. Furthermore, Manabe and Stouffer (1994) obtained an increased freshwater flux of 0.3 Sv poleward of 50°N in a global warming scenario assuming a 1% increase in the concentration of atmospheric CO_2 until a quadrupling of the present value was reached. If the simulated changes in the freshwater fluxes are confined to the Arctic Ocean and the Barents Sea, a doubling to tripling of the present

river runoff of about 0.1 Sv (Aagaard and Carmack, 1989) is obtained.

Based on the scenario-derived estimates of increased surface freshwater flux to the high northern latitudes, idealized model experiments with increased freshwater fluxes to the Arctic region have been conducted.

The three integrations are

CTRL: No change in the freshwater flux.

PX2: Doubling of the freshwater fluxes from the Arctic rivers.

PX5: Fivefold increase in the freshwater fluxes from the Arctic rivers.

Together with the increased surface freshwater fluxes, the thickness of the Arctic sea ice was reduced in the perturbed simulations to mimic an expected sea ice response to global warming (Vinnikov et al., 1999). This was done by introducing the notion of "Arctic warming", where an ad hoc assumption was made that the warming scaled with the added freshwater (see Appendix). The inclusion of the artificial warming in the Arctic led to a reduced sea ice thickness of 1.5–2 m in the central Arctic by year 50 (Figs. 2a, b). These melting rates are comparable to those found in scenario integrations with fully coupled climate models (Vinnikov et al., 1999).

Gradual reductions in the sea ice volume of 3000 km^3 and 3600 km^3 respectively in PX2 and PX5 were obtained over the first 40 years (Fig. 2c). This corresponds to additional freshwater sources of 0.0024 Sv and 0.0030 Sv to the central Arctic Ocean in PX2 and PX5. This is only 2%–3% of the present-day river runoff of 0.1 Sv, and should therefore not be significant compared to the large increases in the river runoff in the perturbed simulations.

It should be noted that a changed climate system will, in general, lead to changes in all of the air-sea ice-ocean fluxes. Moreover, the use of contemporary climatological wind stress is a limitation of the study. Recent observations indicate that the Arctic warming and sea ice melting is related to changes in the atmospheric circulation (Walsh et al., 1996; Thompson and Wallace, 1998). Such changes have not been considered in this study. The presented perturbation integrations should therefore be viewed as idealized sensitivity experiments only.

Finally, the artificial boundary at 20°S will prevent anomalies generated in the northern high latitudes from propagating into the South Atlantic. The closed boundary will therefore have an effect on the dynamics and thermodynamics of the North Atlantic Ocean, at least on long (i.e., multi-decadal) timescales. However, for the relatively short duration of the integrations presented here (50 years) this restriction is most likely not so important (see also the discussion in section 6).

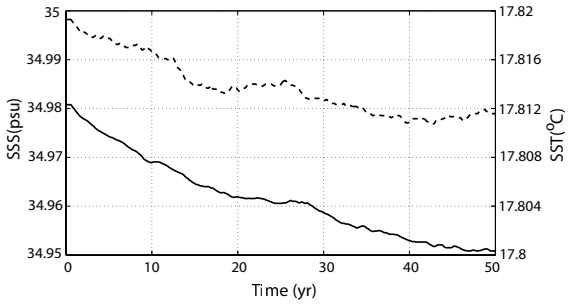

Fig. 3. Time series of the annual mean sea surface salinity (psu; solid line) and sea surface temperature (°C; dashed line) for the model domain in CTRL.

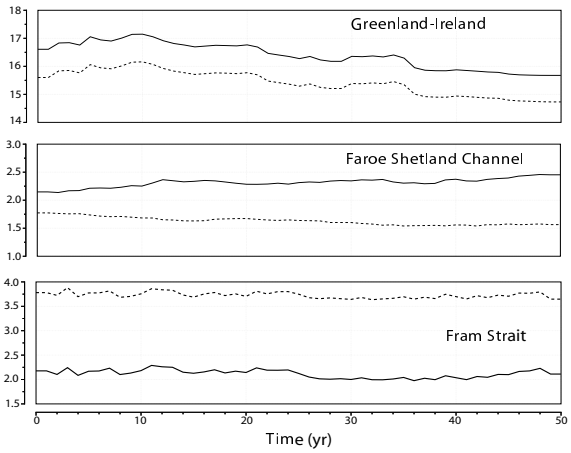

Fig. 4. Time series of the net annual mean northward (solid line) and southward volume transports (Sv) for the Greenland-Ireland section, the Faroe-Shetland Channel, and the Fram Strait in CTRL.

4. The CTRL simulation

Time series of the annual averaged SSS and SST over the entire model domain over the 50-year integration period show relatively small drifts in SSS [0.03 psu (practical salinity-unit)] and SST (0.08°C; Fig. 3). The volume transports through some key passages in the model also remain fairly stable (Fig. 4). However, a reduction in the transports across the Greenland-Ireland section can be noted, as well as a slight increase in the transport over the Faroe-Shetland Channel. This could indicate a slight rearrangement of the splitting of the North Atlantic Drift (NAD) south of Iceland, with relatively more Atlantic water entering the Faroe-Shetland Channel rather than the subpolar gyre. In the Arctic Ocean, the volume transport across the Fram Strait is stable throughout the integration period.

It is also clear that the new equilibrium state will only be reached after several thousand years of integration time. Important transitions in circulation can

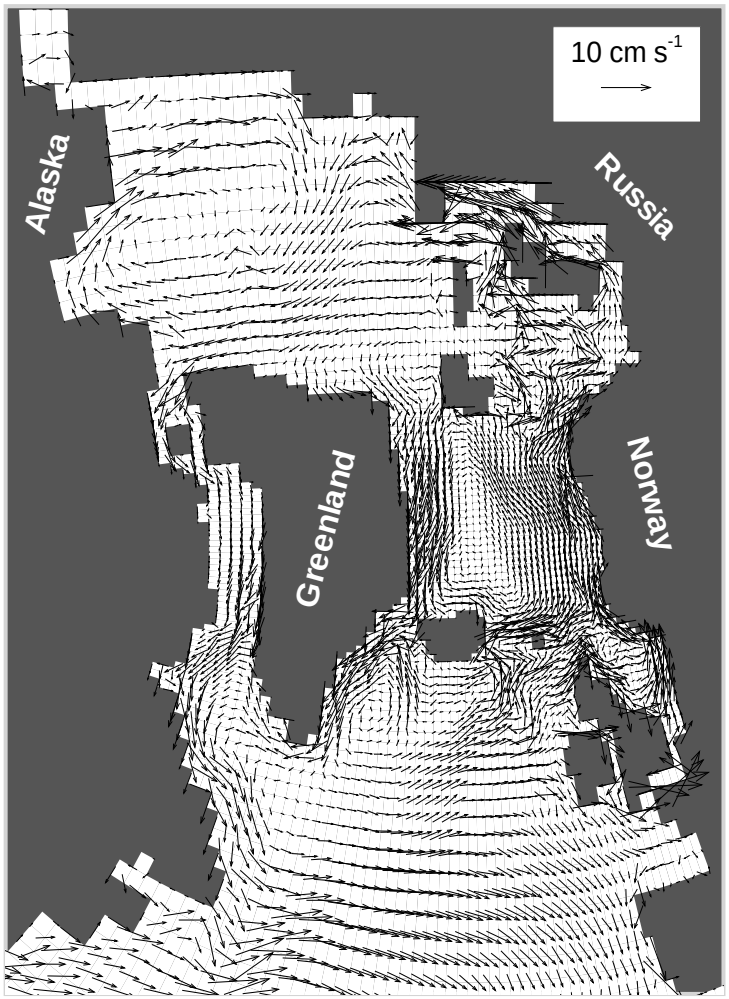

Fig. 5. Simulated annual mean sea surface velocity field (cm s^{-1}) at the start of CTRL.

occur after more than 50 years (Rahmstorf, 1995), even if SST and SSS drifts are slow. An integration period of 50 years is therefore too short to draw any firm conclusions on the model performance. With this shortcoming in mind, CTRL is discussed based on the first year of the simulation.

4.1 *The Arctic Ocean and the Barents Sea*

In the Arctic Ocean, two main features characterize the surface currents (Carmack, 1990). The first is the Transpolar Drift, in which the surface waters of the Eurasian Basin move across the basin towards the North Pole and then towards the Fram Strait. The second is an anticlockwise flow in the Canadian Basin, the so-called Beaufort Gyre. While the Beaufort Gyre seems to be well reproduced by the model, the Transpolar Drift is directed towards the northern part of Greenland rather than the Fram Strait (Fig. 5).

The upper waters of the Arctic Ocean are characterized by a shallow mixed layer at or near the freezing point, overlying a pronounced cold halocline (Rudels et al., 1996). The halocline is a layer with temperatures < -1°C and salinities between 30.4–34.4 psu, leading to a stable vertical density structure in the central Arctic. The model captures a halocline at a depth of about 100–200 m which agrees quite well with observations (Fig. 6).

However, the Atlantic layer is not well reproduced in the model (Fig. 6). For instance, the water at intermediate depths in the Eurasian Basin is too cold (by about 1°C) compared to observations taken during the Oden 91 North Pole Expedition (Anderson et al., 1994). The reason for this is not yet clear, but it could be linked to a too intense cooling, and consequently to a too vigorous surface mixing, in the West Spitsbergen Current south of the Fram Strait in the model.

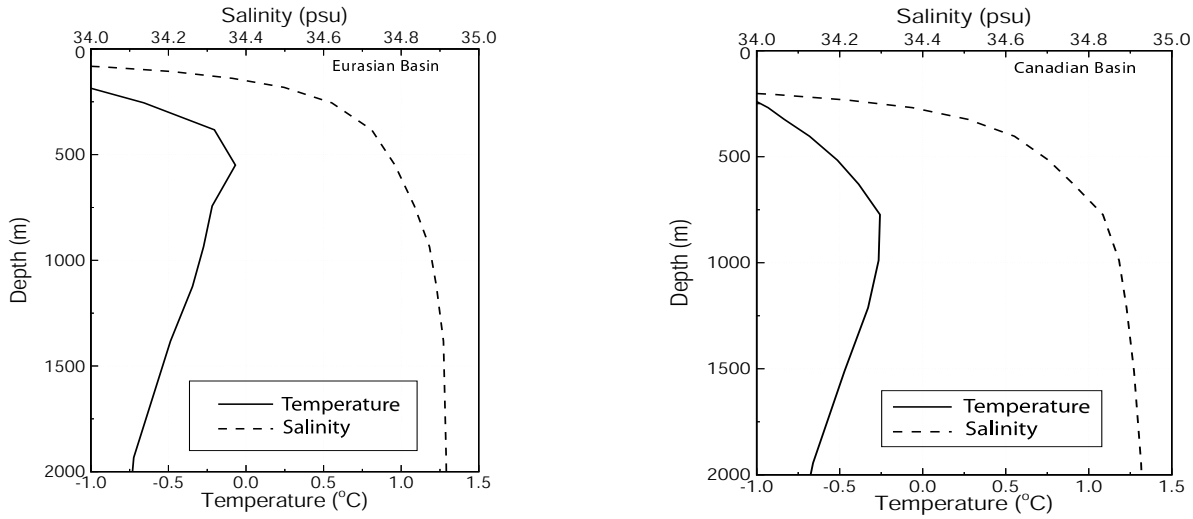

Fig. 6. Modelled vertical temperature and salinity profiles for the Eurasian Basin (left panel) and the Canadian Basin (right panel) (see Fig. 1 for locations).

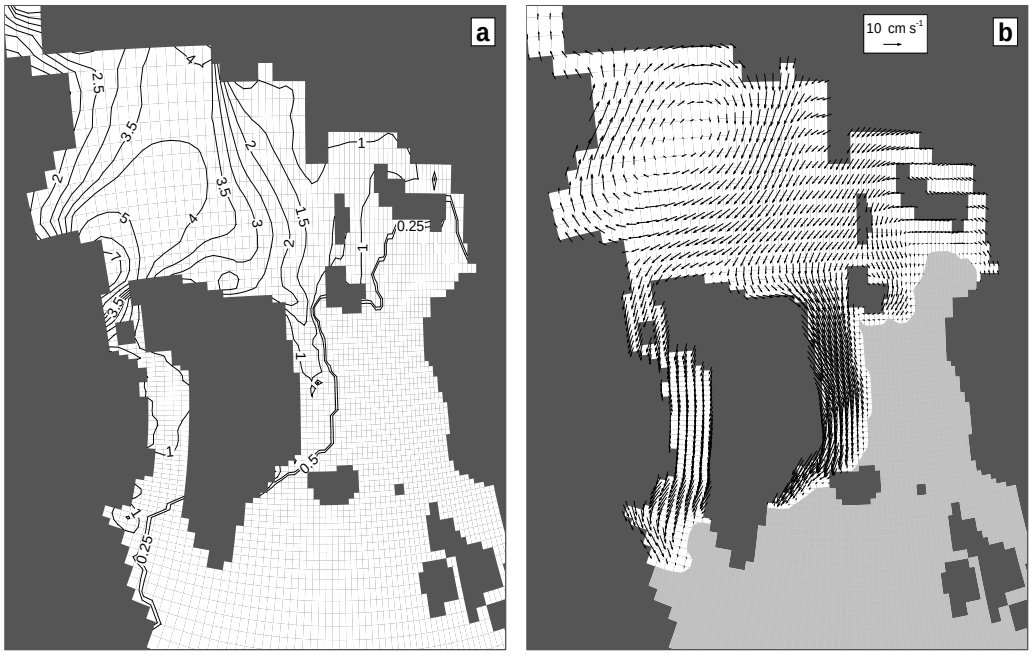

Fig. 7. (a) Sea ice thickness (m) in March at the start of CTRL, and (b) annual mean sea ice velocity (cm s^{-1}) in the first year of CTRL. In panel (a), the contour interval is 0.5 m. In addition the 0.25 m contour level is shown.

The model is able to generate ice cover in fairly good agreement with climatologies derived from observations (Johannessen et al., 1999). In winter, the ice covers all of the Arctic Ocean, the Kara Sea, and the western part of the Barents Sea (Fig. 7a). The maximum sea ice thickness occurs north of Greenland and the Canadian Archipelago, and is in agreement with other studies (e.g., Kreyscher et al., 2000). The sea ice velocity shows a clockwise circulation over the Canadian Basin, and the Transpolar Drift is evident over the Eurasian Basin (Fig. 7b). There is also a drift towards northwestern Greenland and the Canadian Archipelago, leading to the accumulation of ice there.

The exchange of water masses between the Arctic Ocean and the North Atlantic in the model takes place

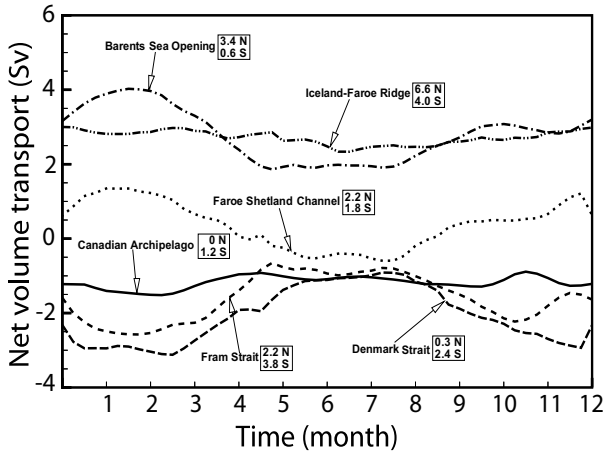

Fig. 8. Total volume transports (Sv) through the major passages in the Nordic Seas and the Arctic Ocean at the start of CTRL. The annual mean northward (N) and southward (S) volume transports are also shown.

through three passages: the Canadian Archipelago, the Fram Strait, and the Barents Sea Opening. The model, as adapted for this study, ignores the inflow of mass and momentum from the Bering Strait, which amounts to about 0.8 Sv based on observations (Roach et al., 1995). The Pacific water carried northwards through this passage is important, since this water ventilates the Arctic Ocean halocline (Roach et al., 1995), with potential consequences for the circulation and sea ice cover in the Arctic Ocean. However, relaxation towards observed annual mean salinity results in realistic sea surface salinity fields for the Bering Strait.

In the model, there is a southward transport of about 1.2 Sv through the Canadian Archipelago and about 1.6 Sv through the Fram Strait (Fig. 8). These fluxes are compensated by a net inflow through the Barents Opening of about 2.8 Sv, yielding a balance of mass for the Arctic Ocean. The obtained water fluxes are in general agreement with observational-based estimates (Simonsen and Haugan, 1996). Some seasonal variation can be seen in the transports through the Fram Strait and the Barents Opening, but not so much in the outflow through the Canadian Archipelago.

4.2 *The Nordic Seas and the northern North Atlantic*

The model reproduces the major current systems in the Nordic Seas and the North Atlantic Ocean (Fig. 5). In the Nordic Seas, two major currents characterize the circulation. These are the Norwegian Atlantic Current in the east, and the East Greenland Current (EGC) in the west, both of which are captured by the model. In addition, a zonal, eastward flow between the EGC and the Norwegian Atlantic Current can be seen northeast of Iceland. All of these currents describe a large cyclonic circulation pattern in the Nordic Seas.

Fig. 9. Mixed layer properties for the Nordic Seas and the northern North Atlantic at the start of CTRL. (a) Annual mean sea surface temperature (°C), (b) annual mean sea surface salinity (psu), and (c) winter mixed layer thickness (m). Contour intervals are (a) 0.5°C, (b) 0.1 psu for contour values $\geqslant$34, and (c) 100 m. In (b) the 32 and 33 psu contour levels are also shown.

In the Labrador Sea, a relatively strong Labrador Current can be seen to flow southward towards Newfoundland. In the Irminger Basin, a branch of the NAD,

the Irminger Current, flows north towards the Denmark Strait where most of it is captured by the strong EGC, thus forming a cyclonic circulation pattern in this area.

Warm and saline Atlantic water (temperature of ∼9–10°C and salinity of about ∼35.1 psu) can be seen to enter the Nordic Seas north of Scotland through the Faroe Shetland Channel (Figs. 9a, b). On its way northwards, the water cools, yielding relatively deep mixed layers in the Greenland, Irminger, and Labrador Seas in winter (Fig. 9c). The model is therefore at least qualitatively able to reproduce the formation of subsurface water masses in these regions. However, in the Labrador Sea, the model seems to underestimate the mixed layer thickness (only about 600 m).

The model produces an inflow of Atlantic water over the Iceland-Faroe Ridge of about 2.6 Sv (Fig. 8). This is in good agreement with an estimate of 2.9 Sv for the Faroe Current based on current measurements (Hansen et al., 1998), but 1.1 Sv below an estimate reported for the Iceland-Faroe Ridge in Hansen and Østerhus (2000). Estimates of the deep overflow through the Faroe Shetland Channel vary between 1.1 and 1.9 Sv in the literature (Simonsen and Haugan, 1996). The model obtains an intermediate and deep overflow of about 1.8 Sv, which is inside this range. The model obtains a total inflow to the Norwegian Sea across the Faroe Shetland Channel of about 2.2 Sv in the surface and intermediate layers (Fig. 8), which is somewhat lower than expected from the most recent observations (Hansen and Østerhus, 2000).

In the Denmark Strait, there is a total southward volume transport of about 2.1 Sv (Fig. 8). Of this, about 0.9 Sv is due to transport in the intermediate and deep layers, while the export with the EGC in the surface is about 1.2 Sv. These estimates are lower than expected from the literature where transport estimates of 3 Sv are found for both the EGC and the deep overflow (Hopkins, 1991). A too coarse grid resolution may be one of the reasons for this.

Despite the commented model deficiencies, CTRL reproduces most of the major features of the modern ocean circulation in the North Atlantic, the Nordic Seas, and the Arctic Ocean, and should therefore provide a fairly realistic framework for the perturbation experiments.

5. The perturbed simulations

5.1 *The Arctic Ocean*

In the Arctic, the major differences in SSS in the freshwater simulations are found downstream of the river discharge areas in Canada, Siberia, and Russia, and after 50 years all of the Arctic Ocean is influenced (Fig. 10). Off the Siberian coast, a clear freshwater belt follows the Transpolar Drift towards Greenland. A large part of this flow enters the Canadian Basin, where it accumulates in the Beaufort Gyre.

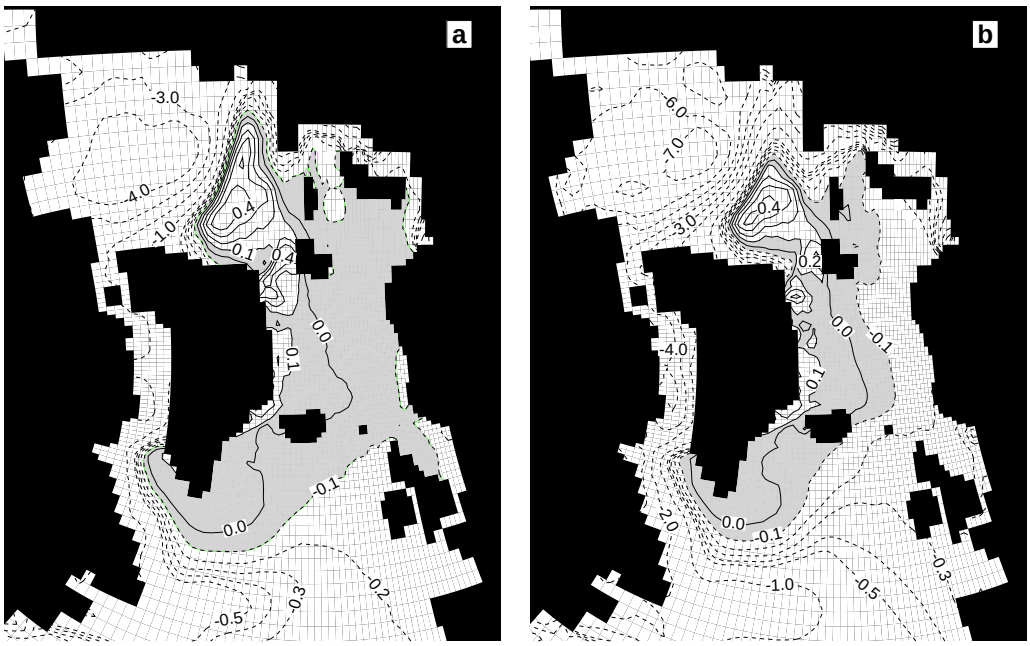

Fig. 10. Difference in annual mean sea surface salinity compared to CTRL in year 50. (a) PX2, and (b) PX5. Dotted lines represent negative anomalies. Contour interval is 1 psu. In addition, the contour lines from −0.5 to 0.5 psu are shown in contour intervals of 0.1 psu.

Fig. 11. Difference in the mixed layer density (in σ_0-units) between CTRL and the perturbed simulations. (a) PX2 and (b) PX5. Contour interval is 0.2 between −1 and 1, and 1 elsewhere. Negative values indicate reduced density.

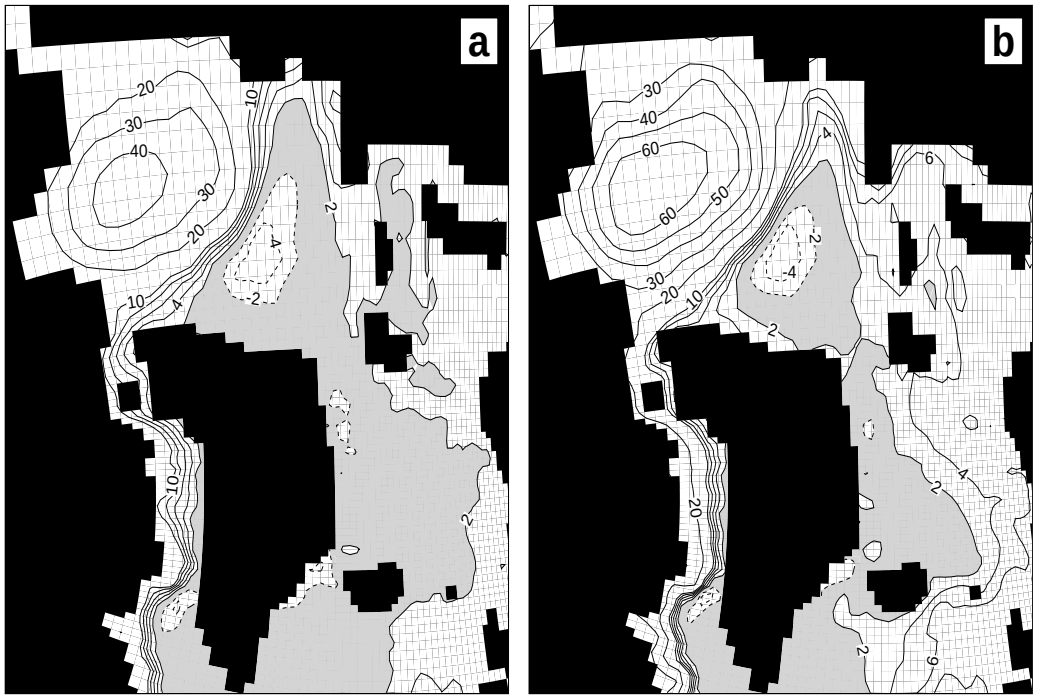

Fig. 12. Difference in sea surface height (cm) between CTRL and the perturbed simulations. (a) PX2 and (b) PX5. Contour interval is 2 cm between −10 to 10, and 10 cm elsewhere.

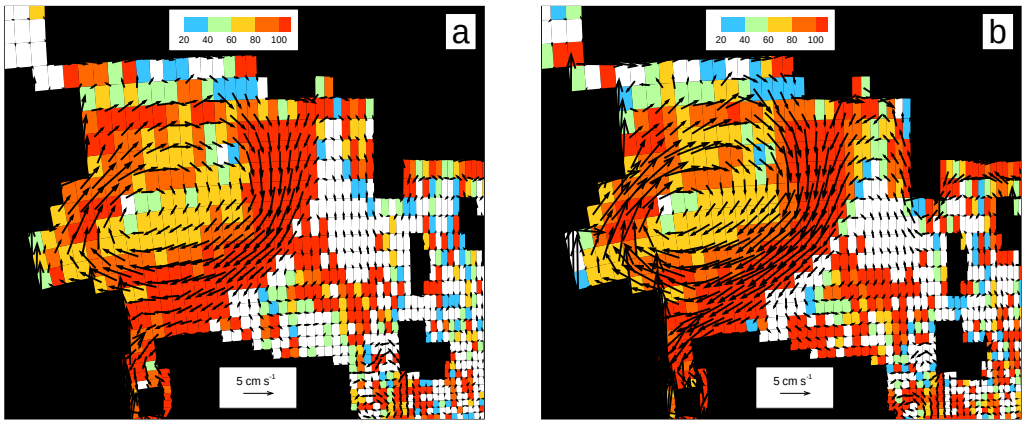

Fig. 13. Difference compared to CTRL in the annual mean geostrophic surface current (cm s^{-1}) in year 50 for (a) PX2 and (b) PX5. The colored shading indicates the relative contribution (in percent) of the increase in absolute geostrophic velocities compared to the absolute total velocities.

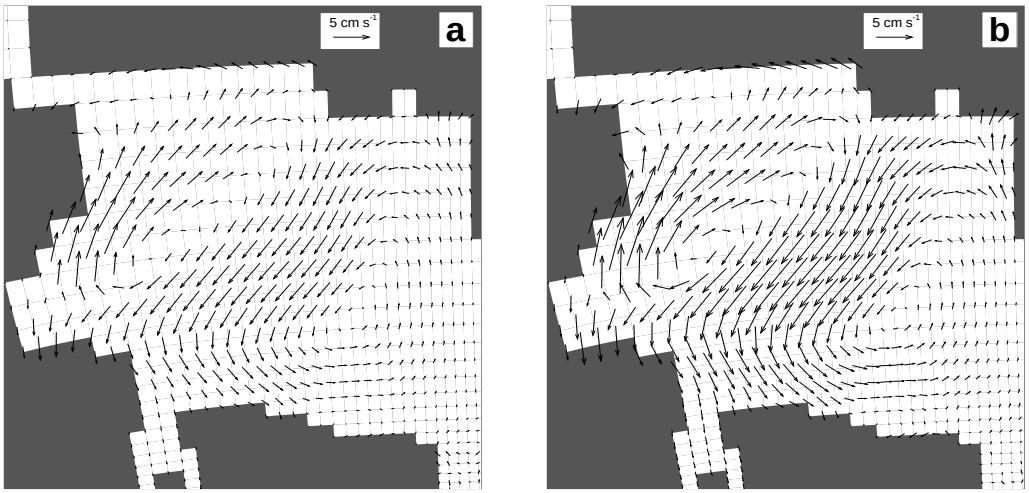

Fig. 14. Difference compared to CTRL in the annual mean sea ice velocity (cm s^{-1}) in year 50 for (a) PX2 and (b) PX5.

Because of the increased freshwater input, a strong density gradient is set up along the periphery of the central Arctic Ocean (Fig. 11). This in turn influences the horizontal pressure gradients, and hence the mixed layer current. Over the Canadian Basin, the sea surface height increases by 40 cm and 60 cm in PX2 and PX5, respectively (Fig. 12).

This in turn induces a relatively strong increase in the geostrophic currents (about 5 cm s^{-1} in the PX5 simulation) in the Beaufort Gyre, leading to an intensified drift towards the Canadian Archipelago (Fig. 13). The changes in the Eurasian Basin are smaller, with the only significant change being an increased drift towards the Laptev Sea in the northern part of the Eurasian Basin.

Furthermore, the artificially reduced sea ice thickness of 1.5–2 m in the central Arctic Ocean also has an impact on the sea ice velocity field (Fig. 14). An increase of about 3–5 cm s^{-1} is found in the Beaufort Gyre. This change is partly attributed to the intensified geostrophic flow (Fig. 13), and partly to the increased momentum transfer through the thinner sea ice.

The simulated change in the sea surface flow field is given in Fig. 15. In PX5, an increase in excess of 6 cm s^{-1} is found in the Beaufort Gyre. A consequence of the changes in the circulation in the Arctic is a gradual increase in the net southward transport through the Canadian Archipelago throughout the whole integration period, reaching almost 0.3 Sv and 0.5 Sv year

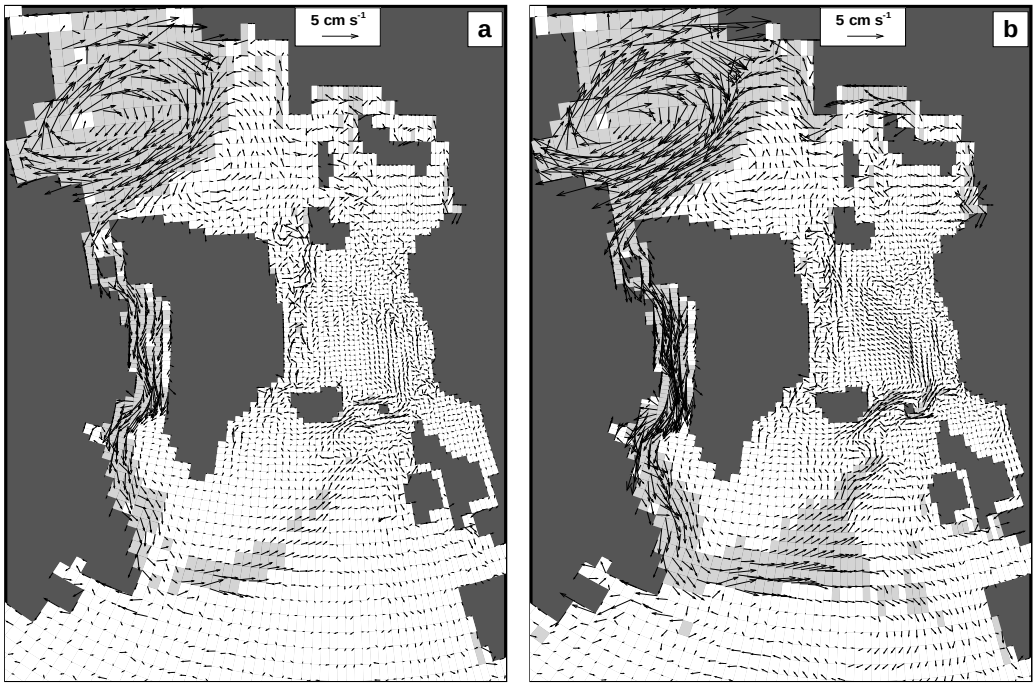

Fig. 15. Difference compared to CTRL in the annual mean surface velocity (cm s^{-1}) in year 50 for (a) PX2 and (b) PX5. Shaded areas indicate an increase in absolute velocity greater than 1 cm s^{-1}.

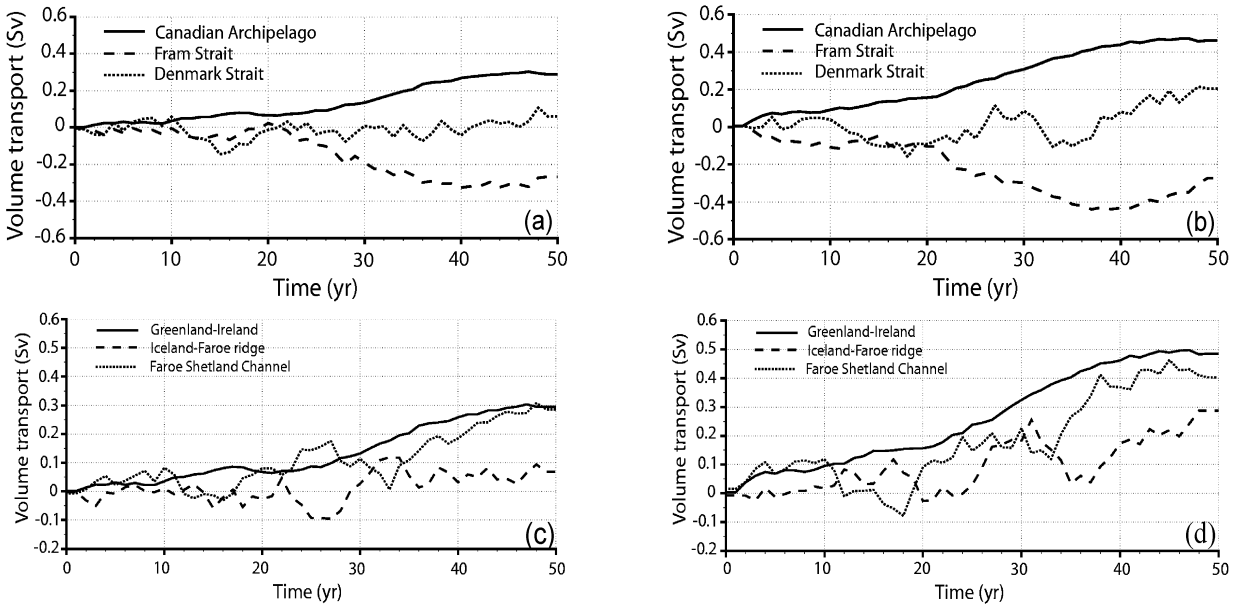

Fig. 16. (a, b) Time series showing the anomaly in the annual mean net southward volume transport (Sv) for PX2 (a) and PX5 (b) through the Canadian Archipelago (solid line), Fram Strait (dashed), and Denmark Strait (dotted). (c, d) Same as in (a, b), but for the annual mean net northward volume transport (Sv) for PX2 (c) and PX5 (d) through the Greenland-Ireland section (solid line), the Iceland-Faroe Ridge (dashed), and the Faroe Shetland Channel (dotted). Negative values indicate reduced transport.

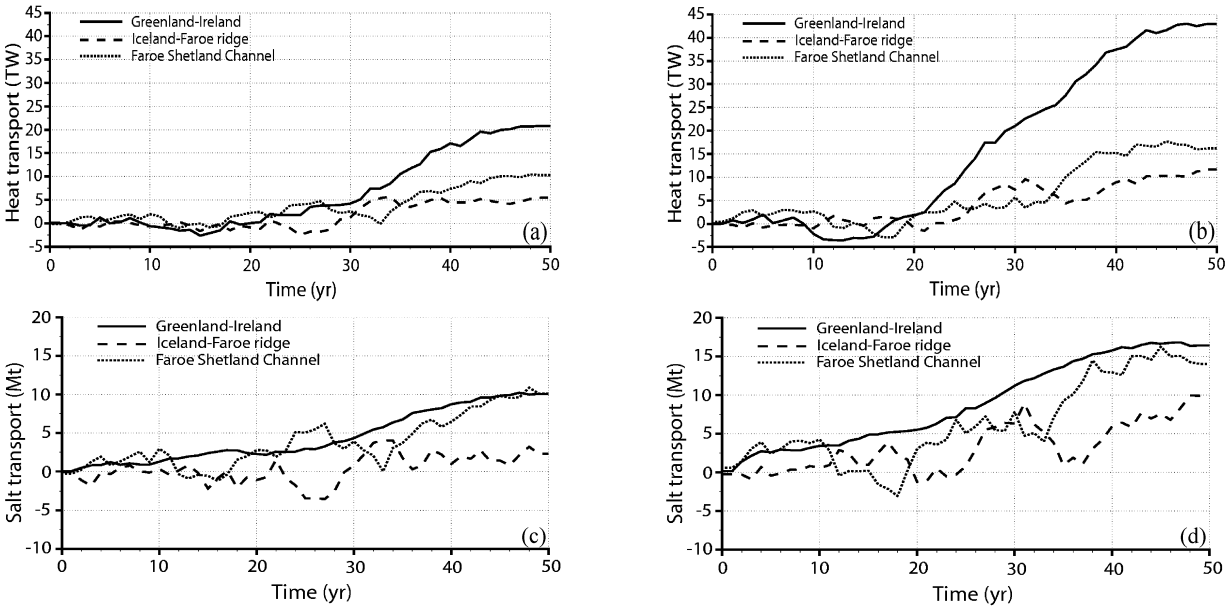

Fig. 17. (a, b) Time series showing the anomaly in the annual mean net northward heat transport (TW) for PX2 (a) and PX5 (b) through the Greenland-Ireland section (solid), the Iceland-Faroe Ridge (dashed), and the Faroe Shetland Channel (dotted). (c, d) Same as for (a, b), but for the annual mean net northward salt transport (Mt) for PX2 (c) and PX5 (d). Negative values indicate reduced transport.

50 in PX2 and PX5, respectively (Figs. 16a, b). The increase in the southward transport is compensated further east through the Fram Strait where the net southward transport is reduced and through the Barents Opening where an increase in the net northward transport is obtained during the last part of the integration (not shown).

5.2 *The Nordic Seas and the northern North Atlantic*

The net northward transport of Atlantic water across the Greenland-Ireland section (see Fig. 1) increases gradually, reaching about 0.3 Sv and 0.5 Sv for PX2 and PX5, respectively (Figs. 16c, d). The increased northward transport thus compensates for the increased southward transport of mass through the Canadian Archipelago.

Most of the change in the northward transport of Atlantic water entering the Nordic Seas takes place in the Faroe Shetland Channel, where increases in the net northward mass transport reach 0.2 Sv and 0.4 Sv in PX2 and PX5, respectively (Figs. 16c, d). As a consequence of this, there is an increase in the supply of both heat and salt to the Nordic Seas through this passage (Fig. 17). The changes in the transports across the Iceland-Faroe Ridge are similar, but smaller than those in the Faroe Shetland Channel. In the Denmark Strait, only minor changes are found in the net volume transport in PX2, while an increased southward transport in excess of 0.2 Sv is seen in PX5.

The simulated mixed layer thickness is the best measure of the formation of sub-surface and abyssal waters in the model. The strongest response to the enhanced freshwater input is found in the Labrador Sea (Fig. 18). The initial response is a rapid decrease in the mixed layer thickness of 110 m and 180 m in PX2 and PX5, respectively (Fig. 18a). However, from year 10 and onwards, a gradual recovery can be seen, leading to an almost complete recovery of the mixed layer in year 50. In the Irminger Sea, the response is much weaker, with a maximum reduction around year 30 of about 40 m and 60 m in PX2 and PX5, respectively, and a slight increase in the mixed layer thickness at the end of the integration (Fig. 18b). In the Greenland Sea, a rapid reduction in the mixed layer thickness of about 30 m and 70 m can be seen between years 10–20 in PX2 and PX5, respectively (Fig. 18c). However, for the rest of the period the mixed layer thickness remains relatively stable.

The reason for the recovery and stabilization of the mixed layer thickness in the Labrador and Greenland Seas is the increased northward transport of Atlantic water with the NAD (Figs. 15 and 16c, d). As a result of the intensified NAD, more salt is transported into these regions (Figs. 17c, d), increasing the density, and by that, compensating for the enhanced freshwater in-

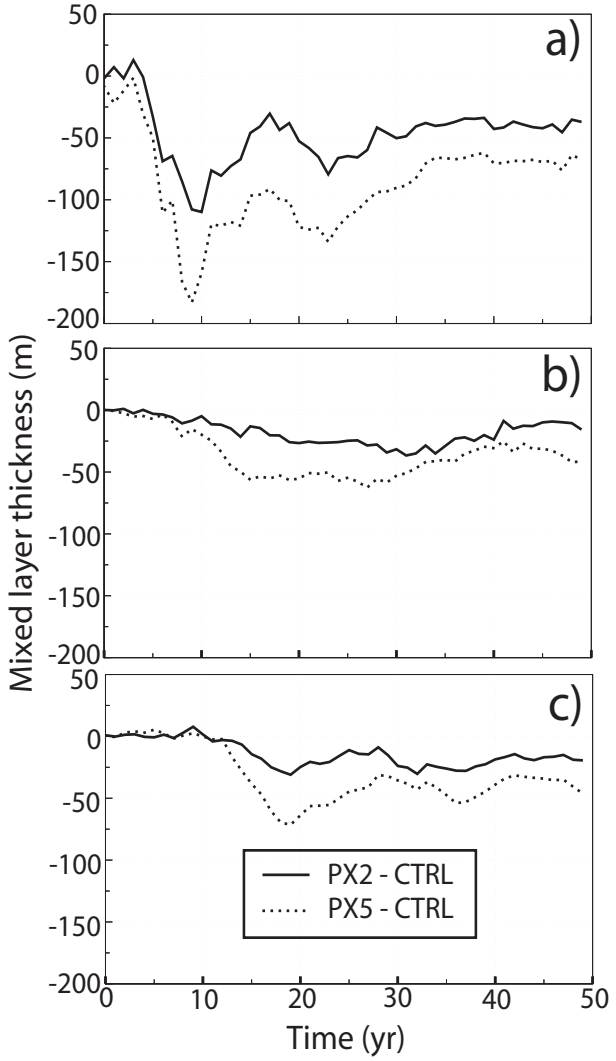

Fig. 18. Time series showing the deviation in the wintertime mixed layer thickness (m) compared to CTRL for PX2 (solid line) and PX5 (dotted line) in the mixing regions of the model domain. (a) Labrador Sea, (b) Irminger Sea, and (c) Greenland Sea.

put from the Arctic.

6. Discussion

The obtained model response indicates that the combined effect of increased freshwater supply to the Arctic Ocean and reduced sea ice thickness tend to have a near stabilizing effect on the NAD. The two feedback mechanisms associated with the response of the NAD to changes in the Arctic river runoff and Arctic sea ice thickness are given in Fig. 19. Firstly, the increased freshwater released in the Arctic Ocean leads to a stabilization of the water column in the Atlantic sub-polar gyre and in the Nordic Seas, resulting in a weakened NAD. Secondly, intensified geostrophic currents due to increased density gradients in the central Arctic Ocean and more efficient transfer of momentum through the thinner sea ice lead to an intensified Beaufort Gyre. The change in the geostrophical currents in the central Arctic is estimated to contribute about 80% of the increased Beaufort Gyre (Fig. 13). The remaining part of the change is caused by the reduced sea ice thickness and the subsequent increase in sea ice velocities in the Beaufort Gyre (Fig. 14). A consequence of these changes is that the southward transport of mass through the Canadian Archipelago increases. Since the Arctic Ocean, the Barents Sea, and the Nordic Seas constitute a closed system (assuming that the flow through the Bering Strait remains fairly constant), this loss of water has to be replaced. In the model, this is accomplished through an intensified NAD, resulting in an ocean state found in CTRL.

Typical climate model responses to global warming scenarios are increased evaporation at low latitudes and increased precipitation, runoff, and glacial melting at high latitudes (Manabe and Stouffer, 1994; Latif et al., 2000; Räisänen, 2001). Some of these models show a substantial reduction in AMOC with possible climatic impacts in northern Europe (e.g., Manabe and Stouffer, 1994; Schiller et al., 1997; Cubasch et al., 2001; Velinga and Wood, 2002). However, in Latif et al. (2000), a different model response is found. Here, large-scale air-sea interactions in the Tropics lead to anomalously high salinities in the Tropical Atlantic. These anomalies are then advected northward into the sinking regions, thereby increasing the surface density and compensating for the effects of the local warming and freshening. An alternative mechanism for maintaining the NAD is operating in the highly idealized model experiments presented here.

The obtained model results further highlight the potential importance of the Canadian Archipelago in controlling the freshwater budget of the Arctic and Atlantic Oceans, and thereby supporting the findings of Goosse et al. (1997). Coarse resolution ice-ocean and climate models are usually set up with a closed Canadian Archipelago (e.g., Prange and Gerdes, 1999; Rahmstorf, 1999). However, several studies (e.g., Agaard and Carmack, 1989; Steele et al., 1996) suggest that the freshwater flux through this passage is larger than the one associated with the freshwater export through the Fram Strait. A closed Canadian Archipelago will force the freshwater to escape through the Fram Strait, and possibly trigger a different ocean response to freshwater scenarios and/or reduced sea ice thickness than the one found in the present study. This underlines the need for representing this passage in global models used in climate studies.

An important limitation of this study is that it has been conducted under prescribed atmospheric conditions, which prevents any feedback mechanisms between the ice-ocean system and the atmosphere. For

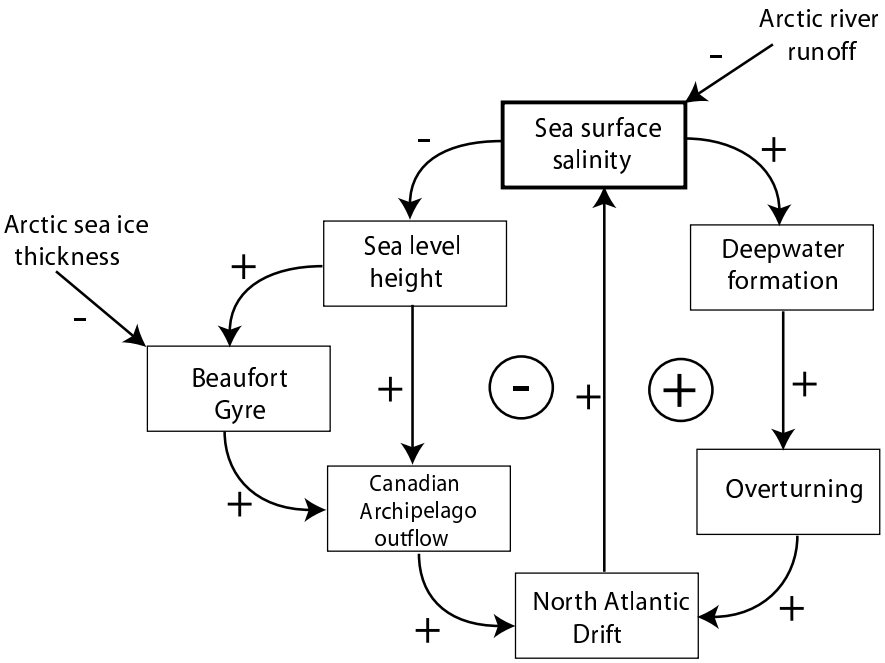

Fig. 19. Schematics of two feedback mechanisms with changes in the NAD in response to changes in the Arctic freshwater budget and sea ice thickness. The signs attached to the arrows indicate the correlation between changes in the quantity of the outgoing box with that of the ingoing box, e.g., increased SSS leads to stronger deep-water formation. The resulting correlations of a loop are circled and they indicate whether a process is self-reinforced (positive sign) or damped (negative sign).

instance, one can expect that a modification of the NAD will affect air temperature and evaporation/precipitation in the Nordic Seas, which in turn may influence the atmosphere-ice-ocean system.

Another limitation of the study is the use of a closed Bering Strait in the model. Since the flow through the Bering Strait is governed by the difference in the sea level height across the strait, it is expected that the flow of Pacific water into the Arctic Ocean will decrease as a consequence of the change in sea level height in the freshwater experiments. Therefore, an open Bering Strait with reduced poleward volume flow will also tend to strengthen the NAD. In fact, in a 150-year twin experiment with the Bergen Climate Model (a fully coupled atmosphere-sea ice-ocean climate model; Furevik et al., 2003), the poleward flow of Pacific water through the Bering Strait decreased, whereas the southward flow through the Canadian Archipelago and the poleward flow through the Faroe-Shetland Channel increased, in response to a three-fold increase in freshwater to the Nordic Seas and the Arctic Ocean (Otterå et al., 2003). These findings support the results presented here.

The present study, although highly idealized and without any form of active atmospheric feedback mechanisms, indicates that increased freshwater supply to the Arctic—also in combination with reduced sea ice thickness in the Arctic—does not necessarily have a one-way negative feedback on the NAD, at least on multi-decadal timescales.

7. Summary

A 3-D isopycnic coordinate OGCM coupled to dynamic and thermodynamic sea ice modules has been used to examine the combined effect of increased freshwater flux to, and reduced sea ice thickness within, the Arctic Ocean. Two 50-year perturbation simulations are examined—one with a doubling of the modern Arctic river runoff, and a second, more extreme case, where the river runoff is five times the modern value. It has been assumed that the additional supply of freshwater follows from a warmer climate. The heat associated with this warming has been applied to the model system by reducing the simulated sea ice thickness.

For both simulations, the modelled ocean response is qualitatively the same: the Arctic and North Atlantic SSS are reduced, leading to an initial weakening of the NAD. The freshening of the surface waters in the Arctic leads to increased density gradients in the central Arctic Ocean. This, together with increased mo-

mentum transfer across the thinner sea ice, leads to an intensified Beaufort Gyre, which in turn increases the volume transport through the Canadian Archipelago. To compensate for this southward transport of mass, more of the warm and saline Atlantic waters are carried northward with the NAD. The increased transport of salt to the northern North Atlantic and the Nordic Seas thus counteracts the impact of the increased freshwater runoff to the Arctic, and tends to stabilize the NAD.

The presented study has focused on the circulation and the thermodynamics of the North Atlantic-Arctic climate system. A continuation of the study is planned with a global coupled atmosphere-ocean model, where the NAD and the AMOC can be studied on centennial timescales. Such studies will be useful to examine theories on glacial circulation, to identify the origin, propagation, and decay of dynamic and thermodynamic anomalies in the Atlantic-Arctic region, and to further explore the role of the flow of water through the Canadian Archipelago in climate studies.

Appendix

Artificially reduced sea ice thickness

Freshwater added to seawater changes the thermodynamic properties of seawater in several ways. If one considers a well mixed surface layer of thickness $h_{\rm ml}$ (m) with temperature $T_{\rm ml}$ (°C) and salinity $S_{\rm ml}$ (psu), the mixed layer temperature and salinity will be modified according to the volumetric expressions

$$S^*_{\rm ml} = \frac{h_{\rm ml}}{h_{\rm ml}+\delta} S_{\rm ml} \ , \quad T^*_{\rm ml} = \frac{h_{\rm ml} T_{\rm ml} + \delta\, T_{\rm fw}}{h_{\rm ml}+\delta}$$

upon addition of δ (m) freshwater with temperature $T_{\rm fw}$ (°C) and vanishing salinity. It should be noted that the freshwater thickness, δ, is just for the theoretical analysis presented here, and is not used in any way in the OGCM experiments described in the text. In the model, the effect of river runoff is parameterized as a virtual salt flux, implying that there is no change in the volume flux at all. Also, for simplicity, the different heat capacities and densities of freshwater and seawater have been ignored in the expression of $T^*_{\rm ml}$.

Through most of the year, $T_{\rm fw} > T_{\rm ml}$ in sea ice covered regions. Therefore, the surface salinity decreases and the surface temperature increases as freshwater is added to the system. It is not given how the modified surface salinity and temperature may influence the growth rate of sea ice since the freezing temperature $T_{\rm f}$ (°C) depends on salinity (Millero, 1978), and since the difference between $T_{\rm fw}$ and $T_{\rm ml}$ is one of the factors that determine the growth rate of sea ice (Drange and Simonsen, 1996).

The modified freezing point of seawater T^*_f can be approximated by the expression

$$T^*_{\rm f} = 0.066 - 0.057 S^*_{\rm ml}$$

for salinities in the range 30–36 psu (Drange and Simonsen, 1996). Since $\delta \ll h_{\rm ml}$, it follows from $\partial S^*_{\rm ml}/\partial\delta$ and $\partial T^*_{\rm ml}/\partial\delta$ that

$$\frac{\partial T^*_{\rm ml}}{\partial S^*_{\rm ml}} = \frac{T_{\rm ml} - T_{\rm fw}}{S_{\rm ml}} \ .$$

In polar regions, the temperature difference $T_{\rm fw} - T_{\rm ml}$ is typically a few °C, and for a surface salinity in the range 30–36 psu, we get that

$$\frac{\partial T^*_{\rm ml}}{\partial S^*_{\rm ml}} \approx -0.06 \ , \quad \frac{\partial T^*_{\rm f}}{\partial S^*_{\rm ml}} = -0.057 \ .$$

Therefore, as a first approximation, the supply of freshwater to ice-covered seawater leads to a change in the surface temperature that is close to the change in the freezing temperature (i.e., $\partial T^*_{\rm ml} \approx \partial T^*_{\rm f}$). The consequences of these considerations are that the supply of freshwater through $S^*_{\rm ml}$ and $T^*_{\rm ml}$ will not, as a first approximation and from a purely thermodynamic point of view, change the growth rate (i.e., thickness) of sea ice despite $T_{\rm fw} > T_{\rm ml}$.

In this study, the warming has been applied to the model system by making an ad hoc assumption that the warming corresponds to the change in $T^*_{\rm ml}$, i.e., to the change in the mixed layer temperature caused by the added freshwater (the warming thus scales with the added freshwater). The heat associated with this warming is then used to melt sea ice from below, leading to a reduced sea ice thickness in the central Arctic as described in Fig. 2.

Acknowledgments. This study has been supported by the Research Council of Norway through Project No. 134542/720 (OHO), the RegClim Project (OHO and HD), and the Program of Supercomputing. Support from the G. C. Rieber Foundation is highly acknowledged. The authors are grateful to the reviewer Peili Wu and an anonymous reviewer for valuable comments on this paper. This is publication No.A73 of the Bjerknes Centre for Climate Research.

REFERENCES

Aagaard, K., and E. C. Carmack, 1989: The role of sea ice and other fresh water in the Arctic circulation. *J. Geophys. Res.*, **94**, 14485–14498.

Anderson, L. G., and Coauthors, 1994: Water masses and circulation in the Eurasian Basin: Results from the Oden 91 expedition. *J. Geophys. Res.,* **99**, 3273–3283.

Arakawa, A, and V. R. Lamb, 1977: Computational design of the basic processes of the UCLA General Circulation Model. *Methods Comput. Phys.* **100**, 174–265.

Aukrust, T., and J. M. Oberhuber, 1995: Modelling of the Greenland, Iceland and Norwegian Seas with a coupled sea ice-mixed layer-isopycnal ocean model. *J Geophys. Res.*, **100**, 4771–4789.

Bleck, R., C. Rooth, D. Hu, and L. T. Smith, 1992: Salinity-driven thermocline transients in a wind- and thermohaline-forced isopycnic coordinate model of the North Atlantic. *J. Phys. Oceanogr.*, **22**, 1486–1505.

Broecker, W. S., W. S. Bond, G. McManus, M. Klas, and E. Clark, 1992: Origin of the North Atlantic's Heinrich events. *Climate Dyn.,* **6**, 265–273.

Carmack, E. C., 1990: Large-scale physical oceanography of polar oceans. *Polar Oceanography, Part A: Physical Science*, W. O. Smith, Ed., Academic Press, Inc., San Diego, California, 171–222.

Clark, P. U., N. G. Pisias, T. F. Stocker, and A. J. Weaver, 2002: The role of the thermohaline circulation in abrupt climate change. *Nature*, **415**, 863–869.

Cooper, C., and C. Gordon, 2002: North Atlantic Ocean decadal variability in the Hadley Centre Coupled Model. *J Climate*, **15**, 45–72.

Cubasch, U., and Coauthors, 2001: Projections of future climate change. *Climate Change 2001: The Scientific Basis*. Contribution of Working Group I to the Third Assesment Report of the Intergovernmental Panel on Climate Change, J. T. Houghton et al., Eds. Cambridge University Press, New York, 526–582.

Drange, H, and K. Simonsen, 1996: Formulation of Air-Sea Fluxes in the ESOP2 Version of MICOM. Tech. Rep. 125, Nansen Environmantal and Remote Sensing Center, Bergen, 24pp.

Dümenil, L. K. Isele, H. J. Liebscher, U. Schröder, and K. Wilke, 1993: Discharge data from 50 selected rivers for GCM validation. Tech. Rep. 100, Max Planck Institute, Hamburg.

ECMWF, 1988: *ECMWF Forecast Model. Physical Parametrization.* Research Manual 3, 2nd Edition.

Fairbanks, R. G., 1989: A 17000-year glacio-eustatic sea level record: Influence of glacial melting rates on the Younger Dryas event and deep-ocean circulation. *Nature*, **342**, 637–642.

Furevik, T., M. Bentsen, H. Drange, I. K. T Kindem, N. G. Kvamstø, and A. Sorteberg, 2003: Description and validation of the Bergen Climate Model: ARPEGE coupled with MICOM. *Climate Dyn.*, **21**, 27–51, doi:10.1007/s00382-003-0317-5.

Gent, P. R., 2001: Will the North Atlantic Ocean thermohaline circulation weaken during the 21st century? *Geophys. Res. Lett.*, **28**, 1023–1026.

Goosse, H, T. Fichefet, and J. H. Campin, 1997: The effects of the water flow through the Canadian Archipelago in a global ice-ocean model. *Geophys. Res. Lett.,* **24**, 1507–1510.

Hansen, B., and S. Østerhus, 2000: North Atlantic-Nordic Seas exchanges. *Prog of Oceanography*, **45**, 109–208.

Hansen, B, S. A. Malmberg, O. H. Saelen, and S. Osterhus, 1998: Measurment of flow north of the Faroe Islands June 1986. ICES Cooperative Research Report No. 225, The ICES NANSEN Project, Copenhagen, 83–95.

Harder, M. 1996: Dynamik, Rauhigkeit und Alter des Meereises in der Arktis. Ph. D. Dissertation, Alfred-Wegner-Institut für Polar- und Meeresforschung, Bremerhaven, 124pp.

Hibler, W. D., 1979: A dynamic thermodynamic sea ice model. *J. Phys. Oceanogr.,* **9**, 815–846.

Hopkins, T. S., 1991: The GIN Sea-A synthesis of its physical oceanography and literature review 1972–1985. *Earth Science Reviews*, **30**, 175–318.

Huschke, R. E., 1969: Arctic cloud statistics from air calibrated surface weather observations. Memo. RM-6173-PR, Rand. Corporation, Santa Monica, Calif, 79pp.

Johannessen, O. M., and M. Miles, 2000: Arctic sea ice and climate change—Will the ice disappear in this century? *Science Prog.*, **83**(3), 209–222.

Johannessen, O. M., E. V. Shalina, and M. Miles, 1999: Satellite evidence for an Arctic sea ice cover in transformation. *Science*, **286**(5446), 1937–1939.

Jones, G. A., and L. D. Keigwin, 1988: Evidence from Fram Strait (78°N) for early deglaciation. *Nature*, **336**, 56–59.

Kreyscher, M., M. Harder, P. Lemke, and G. M. Flato, 2000: Results of the Sea Ice Model Intercomparison Project: Evaluation of sea-ice rheology schemes for use in climate simulations. *J. Geophys. Res.*, **105**, 11299–11320.

Latif, M., 1998: Dynamics of interdecadal variability in coupled ocean-atmosphere models. *J. Climate*, **11**, 602–624.

Latif, M., E. Roeckner, U. Mikolajewicz, and R. Voss, 2000: Tropical stabilization of the thermohaline circulation in a greenhouse warming simulation. *J. Climate*, **13**, 1809–1813.

Legates, D. R., and C. J. Willmott, 1990: Mean seasonal and spatial variability in gauge-corrected, global precipitation. *Int. J. Climatol.*, **10**, 111–127.

Lehman, S. J., and L. D. Keigwin, 1992: Sudden changes in North Atlantic circulation during the last deglaciation. *Nature*, **356**, 757–762.

Levitus, S., and T. P. Boyer, 1994: *World Ocean Atlas 1994*. Volume 4: Temperature. NOAA Atlas NESDIS 4, Washington, D. C., 117pp.

Levitus, S., R. Burgett, and T. P. Boyer, 1994: *World Ocean Atlas 1994*. Volume 3: Salinity, NOAA Atlas NESDIS 3, Washington, D. C., 99pp.

Manabe, S., and R. J. Stouffer, 1994: Multiple-century response of a coupled ocean-atmosphere model to an increase of atmospheric carbon dioxcide. *J. Climate*, **7**, 5–23.

Maykut, G. A., 1978: Energy exchange over young sea ice in the Central Arctic. *J. Geophys Res.*, **83**, 3646–3658.

Millero, F. J., 1978: Freezing point of seawater. Eighth Report on the Joint Panel on Oceanographic Tables and Standards, Annex 6, Paris, UNESCO Tech. Pap. Mar. Sci., No. 28, 29–31.

Mitchell, J. F. B., T. C. Johns, J. M. Gregory, and S. F. B. Tett, 1995: Climate response to increasing levels of greenhouse gases and sulphate aerosols. *Nature*, **376**, 501–504.

Mosby, H., 1962: Water, salt and heat balance of the North Polar Sea and the Norwegian Sea. *Geophys Norv.*, **24**(11), 289–313.

NOAA, 1988: Data Announcement 88-MGG-02, Digital relief of the surface of the Earth. Tech. Rep., NOAA, National Geophysical Data Center, Boulder, CO, U.S.A.

Oberhuber, J. M., 1988: An atlas based on the 'COADS' data set: The budgets of heat, buoyancy and turbulent kinetic energy at the surface of the global ocean. Tech. Rep. Max Planck Institute, Hamburg, 15pp.

Otterå, O. H., H. Drange, M. Bentsen, N. C. Kvamstø, and D. Jiang, 2003: The sensitivity of the present day Atlantic meridional overturning circulation to freshwater forcing. *Geophys. Res. Lett.*, **30**(17), 1898, doi:101029/2003GL017578.

Peltier, W. R., 1994: Ice age paleotopography. *Science*, **265**, 195–201.

Peterson, B. J., R. M. Holmes, J. M. McClelland, C. J. Vorosmarty, R. B. Lammers, A. I. Shiklomanov, I. A. Shiklomanov, and S. Rahmstorf, 2002: Increasing river discharge to the Arctic Ocean. *Science*, **298**(5601), 2171–2173.

Prange, M., and R. Gerdes, 1999: Influence of Arctic river runoff on the circulation in the Arctic Ocean, the Nordic Seas and the North Atlantic. ICES ASC Council Meeting L/11, 5pp

Rahmstorf, S., 1995: Climate drift in an ocean model coupled to a simple, perfectly matched atmosphere. *Climate Dyn.*, **11**, 447–458.

Rahmstorf, S., 1999: Long-term global warming scenarios computed with an efficient coupled climate model. *Climatic Change*, **43**, 353–367.

Räisänen, J., 2001: CO_2-induced climate change in the Arctic area in the CMIP2 experiments. *SWECLIM Newsletter*, **11**, 23–28.

Roach, A. T., Aagaard, K., C. H. Pease, S. A. Salo, T. Weingartner, V. Pavlov, and M. Kulakov, 1995: Direct measurements of transport and water properties through the Bering Strait. *J. Geophys. Res.,* **100**, 18443–18457.

Roullet, G., and G. Madec, 2000: Salt conservation, free surface, and varying levels: a new formulation for ocean general circulation models. *J. Geophys. Res.*, **105**, 23927–23942.

Rudels, B., L. G. Anderson, and E. P. Jones, 1996: Formation and evolution of the surface mixed layer and halocline in the Arctic Ocean. *J. Geophys. Res.*, **101**, 8807–8821.

Schiller, A., U. Mikolajewicz, and R. Voss, 1997: The stability of the North Atlantic thermohaline circulation in a coupled ocean-atmosphere general circulation model. *Climate Dyn.*, **13**, 325–347.

Semtner, A. J., 1987: A numerical study of the sea ice and ocean circulation in the Arctic. *J. Phys. Oceanogr.*, **17**, 1077–1099.

Simonsen, K., 1996: Heatbudgets and freshwater forcing of the Nordic Seas and the

Artic Ocean. Ph. D. Dissertation, Nansen Env. and Remote Sensing Center,

Simonsen, K., and P. M. Haugan, 1996: Heat budgets of the Arctic Mediterranean and sea surface heat flux parametrizations for the Nordic Seas. *J. Geophys. Res.*, **101**, 6553–6576.

Simonsen, K., and H. Drange, 1997: Surface forcing and initialization of the ESOP2 version of MICOM. Tech. Rep. 116, Nansen Environmantal and Remote Sensing Center, Bergen, 28pp.

Steele, M., D. Thomas, and D. Rorhrock, 1996: A simple model study of the Arctic Ocean freshwater balance, 1979-1985. *J. Geophys. Res.*, **101**, 20833–20848.

Sun, S., and R. Bleck, 2001: Atlantic Thermohaline Circulation and its Response to Increasing CO_2 in a Coupled Atmosphere-Ocean Model. *Geophys. Res. Lett.*, **28**, 4223–4226.

Thompson, D. W. J., and J. M. Wallace, 1998: The Arctic Oscillation signature in the wintertime geopotential height and temperature fields. *Geophys. Res. Lett.*, **25**, 1297–1300.

Timmermann, A., M. Latif, R. Voss, and A Grötzner, 1998: Northern Hemispheric interdecadal variability: A coupled air-sea mode. *J. Climate*, **11**, 1906–1931.

Vellinga, M., and R. A. Wood, 2002: Global climatic impacts of a collapse of the Atlantic thermohaline circulation. *Climatic Change*, **54**, 251–267.

Vinnikov, K. Y., and Coauthors, 1999: Global warming and Northern Hemisphere ice extent. *Science*, **286**, 1934–1937.

Walsh, J. E., and C. M. Johnson, 1979: An analysis of Arctic ice fluctuations, 1953–77. *J. Geophys. Res.*, **9**, 580–591.

Walsh, J. E., W. L. Chapman, and T. L. Shy, 1996: Recent decrease of sea level pressure in the Central Arctic. *J Climate*, **9**, 480–486.